ACADEMIA ROMÂNĂ
Revue Roumaine de Chimie
http://web.icf.ro/rrch/

Rev. Roum. Chim.,
2014, *59*(2), 151-159

FORMATION BY LASER ABLATION IN LIQUID (LAL) AND CHARACTERIZATION OF CITRIC ACID-COATED IRON OXIDE NANOPARTICLES

Anamaria DURDUREANU-ANGHELUTA,[a] Claudia MIHESAN,[a,*] Florica DOROFTEI,[a] Andrei DASCALU,[a] Laura URSU,[a] Michalis VELEGRAKIS[b] and Mariana PINTEALA[a]

[a] Centre of Advanced Research in Bionanoconjugates and Biopolymers, "Petru Poni" Institute of Macromolecular Chemistry of Roumanian Academy, 41A Grigore Ghica Voda Alley, 700487 Iaşi, Roumania
[b] Institute of Electronic Structure and Laser, FORTH, Heraklion 71110, Crete, Greece

Received January 30, 2014

This work presents the synthesis of magnetic nanoparticles coated with a hydrophilic shell of citric acid, by a one-step technique based on laser ablation in liquid. The obtained nanoparticles were characterized in terms of size distribution and stability by DLS and microscopic techniques; the morphology was investigated using HRTEM and the surface chemistry was studied by XPS technique and FTIR spectroscopy. The results show the formation of stable spherical nanoparticles, having a single size distribution centered around 60 nm. The nanoparticles are composed of an iron oxides core, stabilized by a citric acid coating.

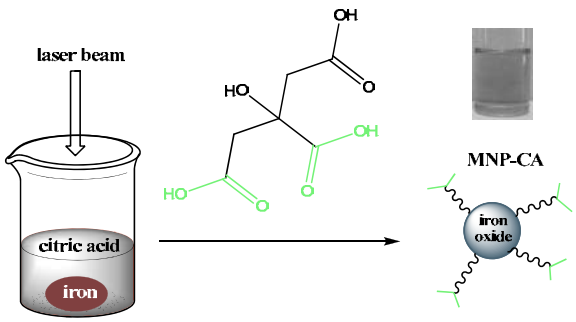

INTRODUCTION

Magnetic nanoparticles (MNPs) are considered to be a "hot" topic for many researchers due to their specific characteristics: superparamagnetism, colloidal stability, biocompatibility and low toxicity, making them especially interesting for a large series of applications. Therefore, several chemical and physical methods have been developed for production of magnetic iron oxide nanoparticles.[1-5]

By conjugating the magnetic nanoparticles with various molecules of biological interest (protein, DNA, biotin, folate, etc.), the resulting composite nanomaterials (bionanoconjugates) are especially useful for application in biomedicine.[1,3-5] Nano-bioconjugates consist of two main components: a nanonucleus (fullerene, cyclodextrin, magnetite, gold, etc.) functionalized with a reactive group at the end of a spacer chain (forming together the nanoconjugate) and a biomolecule, attached by ionic or hydrogen bonds, to the nanoconjugate.[6] For example, hydrophilic core-shell magnetite particles were obtained by interchanging the shell formed by oleic acid with 3-aminopropyltriethoxysilane, a suitable reactive compound for subsequent conjugation with biomolecules.[7-9]

Another route to obtaining coated nanoparticles is the laser ablation in liquid (LAL).[10-14] The

* Corresponding author: claudia.mihesan@icmpp.ro

interaction of a highly energetic laser beam (usually pulsed) with a solid material leads to the material disintegration and vaporization, forming a gaseous plasma containing atoms, molecules, ions, excited species, clusters, nanodroplets of melted material, etc. called the ablation plume. By rapidly quenching the laser ablation plume (in case of LAL), new compounds can be synthesized by reactions between species in the plasma or between plasma and compounds of the liquid phase and new materials are formed as particles, suspended in the liquid phase (in the ablation medium).

The nanoparticles (NPs) formation by LAL has several advantages over the widely used chemical methods. The chemical syntheses usually rely on a complicated protocol and are sensitive to a variety of parameters of the experimental procedure (*i.e.* concentration, pH, presence/absence of oxygen temperature or pressure variation, impurities that could act as catalysts, side reactions, byproducts formation etc.). The chemical methods, especially for metastable phase synthesis, require high temperature and pressure, quite difficult to achieve in chemical reactors. In contrast, high pressure-high temperature conditions are easier obtained in a much localized volume by LAL. Over the chemical methods for synthesizing nanoparticles, the LAL has the main advantage of being a straightforward method, producing particles starting from simple and easily available materials, without using any (potentially toxic or very expensive) catalysts. Moreover, the nanoparticles obtained are "clean" and as a direct consequence, no time consuming (or prone to losses) purification is needed; the nanoparticles are "ready to use" either directly for biological applications or for subsequent conjugation with various molecules of interest. More importantly, the LAL offers the possibility of adjusting the size, composition and even shape of the particles by tuning the lasers parameters, the target or the solution composition.[15] The main disadvantage arises from the still limited understanding of the formation mechanisms and of the influence (individual or combined) of any of these parameters. Limited amount of nanoparticles are produced by this method, making more difficult the products' characterization.

The above-mentioned characteristics of LAL make it a very popular method for obtaining NPs, as illustrated by the several recent reviews on the subject[10-13] and more particularly on metal oxide based nanomaterials.[14]

It has been shown that laser ablation of metallic iron in water produces a metastable form of iron oxide (FeO) at the surface of the target.[16, 17] Further irradiation of the oxidized iron under water forms FeO and spinel Fe_3O_4 phase.[18] Laser ablation of metallic iron in water or aqueous solution is a straightforward method to obtain iron oxide nanoparticles with adjustable properties. For example, poly(vinylpyrrolidone)-covered FeO nanoparticles with different sizes were produced by varying the surfactant concentration in the liquid phase.[15] Surfactant free iron oxide nanoparticles with good magnetic properties and biological applications were obtained by laser ablation in water with laser irradiation at 1064 nm[19] and the size distribution, crystallinity and magnetite fraction were improved by subsequent irradiation at 355 nm.[20]

Ablation of iron in different solvents[21,22] has been shown to form nanoparticles with different chemical phases (carbide, oxide, metal and metal-oxide) and/or different nanostructures.[23,24] The composition of the NPs can be varied by using a composite target[25] or different precursors in the liquid phase.[26]

In order to produce metallic Fe nanoparticles, the oxidation of the formed NPs can be avoided using a liquid with high H^+ concentration [27] or by passing gaseous hydrogen through the liquid before and during the laser ablation.[28] By using a longer laser pulse (*i.e.* milisecond) the energy is not enough to create a plasma and the ejected melted nanodroplets are not completely oxidized and therefore Fe/Fe_xO_y core/shell nanospheres are obtained.[29, 30]

In this paper, we present the formation of magnetic nanoparticles by laser ablation of Fe in aqueous solution of citric acid. Citric acid is known to stabilize an aqueous dispersion of magnetite nanoparticles[31,32] and due to steric reasons there is a high probability of having one or two of the three carboxylic groups free for subsequent reactions in the liquid medium, allowing thus further functionalization.[33,34] The obtained nanoparticles were subsequently characterized in terms of stability and size using different standard techniques, such as UV-Vis spectroscopy, Dynamic Light Scattering (DLS), Scanning Electron Microscopy (SEM), Transmission Electron Microscope (TEM), Atomic Force Microscopy (AFM). Information regarding the chemical composition was obtained using X-Ray Photoelectron Spectroscopy (XPS) and Fourier Transform Infrared Spectroscopy (FTIR).

EXPERIMENTAL

Nanoparticles Synthesis by LAL. The laser beam used for nanoparticles synthesis is the fundamental of a Q-switched Nd:YAG laser (BM Industries, series 5000), at 1074 nm, pulse duration 7 ns and 10 Hz repetition rate. A spherical lens with f=20 cm was used to partially focus the beam and the target was placed before the focal point, so as the beam diameter on the sample was 3 mm and the energy density (fluence) on the surface was 1.1 J/cm^2.

The target (iron plate, 1 mm thickness, Goodfellow) is immersed in 2 ml of 0.05 w% aqueous citric acid (Sigma Aldrich) solution and irradiated for 20 minutes. A similar experiment was performed in the absence of citric acid, but the particles obtained in pure water were very unstable and agglomerated quickly, preventing their analysis. In both cases, magnetic nanoparticles were produced, as proved by their migration in the presence of a magnet placed in their vicinity.

Dynamic Light Scattering. The hydrodynamic diameter and Zeta potential of the nanoparticles were evaluated using Delsa Nano C Submicron Particle Size Analyzer (Beckman Coulter, Inc., Fullerton, CA). This device is equipped with a laser diode operating at 658 nm. Measurements were made at room temperature in flow cell for both size and Zeta potential, after the solution was dispersed by ultrasonication.

Optical Absorption. The UV-Vis absorption spectra were measured in the range of 200-800 nm, using a quartz cuvette (Hellma Analytics) with 2 mm optical path, on a Lambda 950 UV-Vis Spectrometer (Perkin Elmer).

Atomic Force Microscopy. The AFM measurements were performed using a Ntegra Spectra – NT-MDT, Russia instrument operated in tapping mode, under ambient conditions. Silicon cantilever tips (NSG 10) with a resonance frequency of 140-390 kHz, a force constant of 5.5-22.5 Nm^{-1} and tip curvature radius of 10 nm were used. The scan rate was 0.5 Hz. To prepare samples for AFM measurements, 10 µl of nanoparticle suspension were deposited on freshly cleaved mica substrates and dried in air at room temperature.

Electron Microscopy. Morphological studies of produced nanoparticles were performed using a scanning electron microscope (SEM) (Quanta 200-FEI) and a transmission electron microscope (TEM) (Hitachi HT7700). Environmental scanning electron microscopy (ESEM) was used in order to determine the morphology, size and elemental composition of the samples. Scandium – Olympus Soft Imaging was used to measure the size distribution from SEM images. The Quanta 200 scanning electron microscope equipped with an energy-dispersive X-ray spectroscopy (EDX) system allows quantitative and qualitative compositional analysis. Particles size, shape and degree of crystallinity were analyzed by transmission electron microscopy.

Samples preparation for SEM: In order to prepare samples for scanning electron microscopy a drop of MNP-CA dispersion in water was deposited on a microscope glass and then dried for 48 hours in an oven at 40ºC. At this temperature, no physical or chemical modification of the nanoparticles is expected. Double-sided carbon tape was used to mount the samples on aluminum stubs and were coated with a 5 nm gold layer using a Leica EM SCD 005 sputter. SEM investigations were performed in high vacuum mode using a secondary electron detector at accelerating voltage of 30 kV.

Sample preparation for TEM: The sample was dispersed by ultrasonification in water and one drop of this solution was placed on a carbon-coated grid leaving the solvent to evaporate in an oven at 40°C for 72 hours. After drying, the samples were examined using a Hitachi HT7700 microscope operating at 100 kV in High Resolution and Diffraction mode.

X-Ray Photoelectron Spectroscopy. X-ray photoelectron spectrometry analysis was performed using an Axis Nova spectrometer (Kratos Analytical Ltd.). The pressure in the analysis chamber was typically 3x10^{-9} mbar. The elemental composition was obtained from the survey spectra (pass energy of 160 eV), while high-resolution spectra were collected with a pass energy of 20 eV. All binding energies were referenced to the C 1s peak at 285 eV. The intensities were calculated from the peak areas using Vision Processing software (Vision2 software, Version 2.2.10). The samples were prepared by dropwise addition of the particles suspension on a microscopy glass and solvent evaporation under nitrogen flow at room temperature.

Fourier Transform Infrared Spectroscopy. The infrared spectra were recorded using a Bruker Vertex 70 FTIR instrument, in transmission mode, in the 400–4000 cm^{-1} range (resolution 2 cm^{-1}, 32 scans), at ambient temperature, in KBr pellet. The FTIR sample was prepared by pipetting a few microliters of nanoparticles solution on a KBr pellet and allowing it to dry in an oven, under vacuum, at 40 ºC, for 2 hours.

RESULTS AND DISCUSSION

Optical Absorption

During the laser irradiation of the Fe plate immersed in the transparent citric acid solution, a change of color was observed. In order to identify the origin of the color change, firstly, the UV-Vis absorption was used to assess possible modifications of the citric acid solution by laser irradiation. The absorption spectra of a Fe-free sample before and after irradiation with the same laser parameters (wavelength, laser energy, number of pulses, repetition rate) as those used for nanoparticles production are identical (not shown), therefore it is safe to assume that no chemical change is induced by laser-citric acid interaction, and all subsequent optical modifications are due to nanoparticles formation. The Fe-free citric acid aqueous solution is transparent in the visible domain, but has a UV band, starting at around 240 nm. However, laser ablation of a solid sample is a very energetic process, the local temperatures attained at the plasma plume-liquid interface could induce some chemical modifications of the organic molecule[35] but in our case, no such decomposition products were detected by XPS analysis (see "Surface chemistry analyzed by X-ray photoelectron spectroscopy (XPS) section").

The progressive formation of nanoparticles in the liquid is indicated by the change in color of the initially transparent solution. As expected, the liquid containing the laser-irradiated Fe, becomes

more yellowish with increasing exposure time[36] and laser fluence.[37] Contrary to similar attempts,[19] in our case, the particles obtained in the absence of citric acid (in pure water) agglomerated and were deposed at the bottom of the vial within minutes following their synthesis. Their reddish color indicated the formation of fully oxidized Fe_2O_3 or the presence of larger particles, while the NP colloids obtained in citric acid solutions are more yellowish and stable for weeks.

Fig. 1(a) shows the absorption spectrum of colloid obtained by laser ablation of Fe in citric acid solution at 1.1 J/cm^2 (dashed line). The absorption of initial citric acid solution is also shown (dotted line) and the difference of the two spectra (full line) is indicative for the nanoparticles formed.

The colloid has a strong extinction in UV, becoming almost transparent for λ>450 nm. This can be explained by Mie theory; our spectrum is similar to the calculated scattering of 10 nm Fe particles in water and in vacuum.[38] The small shoulder at around 255 nm can be correlated either with the presence of Fe^{3+} /citrate complex[39] or with the plasmon resonance of the nanoparticles. For particles slightly smaller than ours, the plasmon resonance is at 270 nm,[28] and the red shift compared with the calculations was explained by the presence of oxide.

Dynamic Light Scattering

Size analysis (Fig. 1(b)) indicates that only a single population of nanoparticles is present in the as-prepared colloids, with a mean diameter of 40 nm. Comparable size distributions were obtained by TEM and AFM microscopy (See Table 1).

In order to characterize the stability of NPs, we measured the Zeta potential of the solution. The obtained negative value (-54.71mV) is large enough to prevent particles agglomeration by electrostatic repulsion and confirms the very good stability of our colloidal dispersion.

AFM characterization

The AFM images of nanoparticles obtained in the presence of citric acid are shown in Fig 2(a,b). The measured mean size is ~62 nm with a standard deviation of 22 nm (fig 2(c)), in agreement with DLS results. The visible agglomeration of nanoparticles is most likely caused by the solvent evaporation during sample preparation.

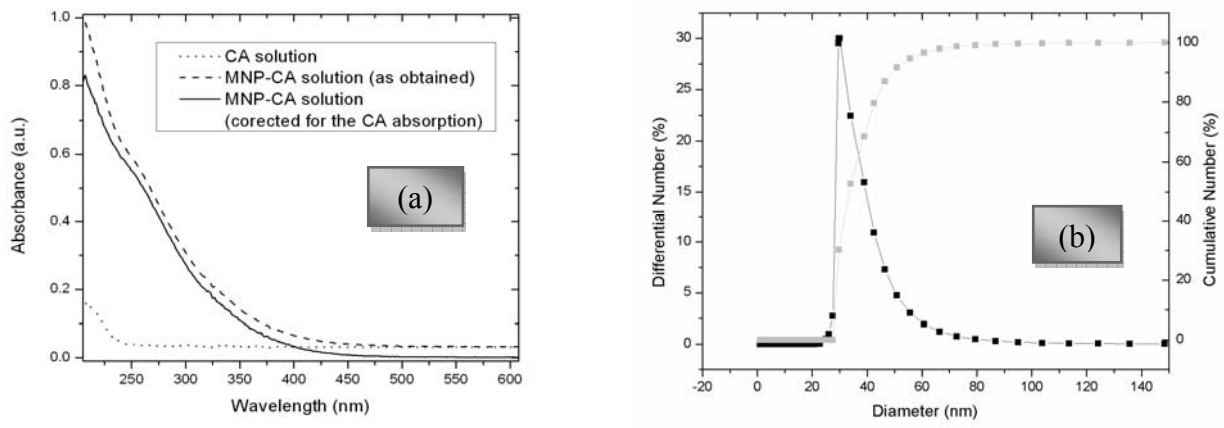

Fig. 1 – (a) UV-Vis absorption spectra; (b) DLS analysis of MNP-CA obtained by laser ablation of Fe in citric acid solution.

Table 1

Diameter measured by different methods

Technique	MNP-CA diameter (nm)
DLS	40
AFM	62
SEM	40-100
TEM	40-70

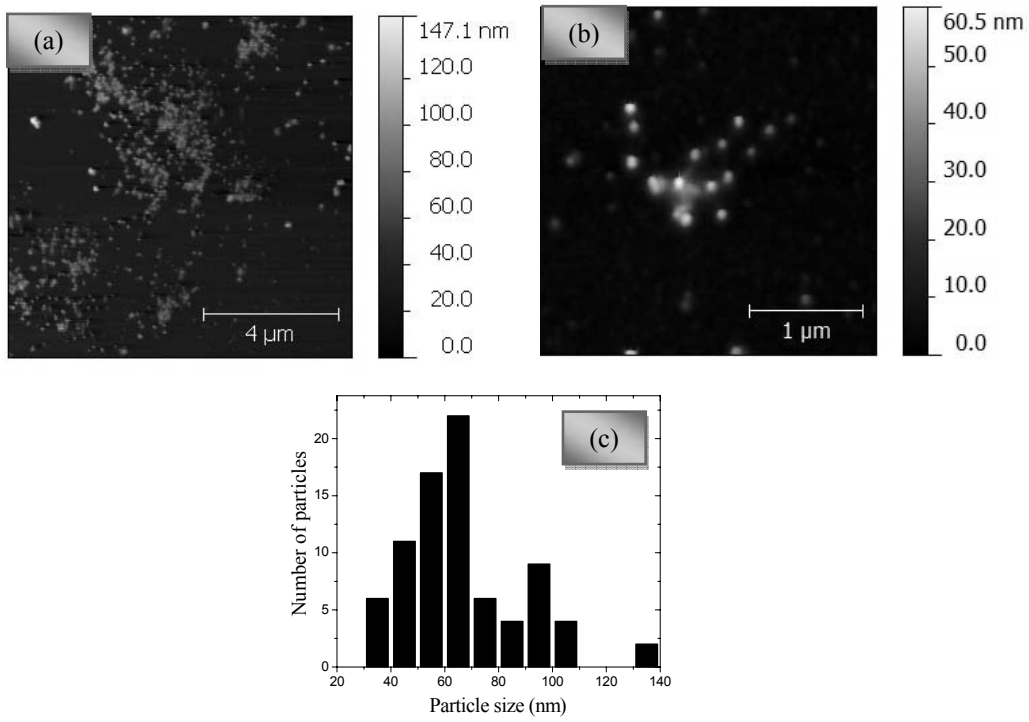

Fig. 2 – (a,b) AFM images of magnetic nanoparticles obtained in the presence of citric acid. Scan size: 10x10 and 3x3 micron. (c) Size distribution of NPs, as measured by AFM.

SEM and EDX analysis

Two SEM images of the sample are shown in Fig. 3(a,b). From the SEM micrographs, it can be observed that all particles have spherical shape, with a size distribution between 40-100 nm.

The EDX analysis shows the presence of elements of the precursors, respectively Fe, C, and O (Fig. 3(c)), and the other identified elements (Si, N, F, K) arise from the glass sample substrate. For a better precision of element identification we used point analyses on different particles. Working at same accelerating voltage, the percentage of Fe varies for different particles, due to different degree of citric acid coverage, particle dimension and density. The results show a good correspondence with the XPS analysis, in the limit of experimental errors and sample inhomogeneity (See Table 2).

TEM characterization

The particle-size distribution and morphology have been examined by TEM imaging. Fig. 4(a,b) show the TEM micrograph of MNP-CA while the inset 4(c) presents the diffraction pattern. The nanoparticles have a roughly spherical shape, diameter ranging from 40 to 70 nm, with an average value of approximately 60 nm. It can be clearly seen from Fig. 4 (a,b) that some of MNP-CA particles have a multicore structure. The cores (approximately 5 nm diameter) have higher electron density (black color on the picture), compared with the outer gray layer, with an average thickness of about 35 nm. The presence of the aqueous medium and high reactivity of laser ablated Fe leads to the formation of nanoparticles covered in oxide shell.[15,19,20,27-29] The presence of intense and sharp spots in the electron diffraction (ED) pattern (see Fig. 4(c)) indicates high crystallinity and crystal order of the sample.

Surface chemistry analyzed by X-ray photoelectron spectroscopy (XPS)

XPS analysis was used to determine the presence of iron oxides in the studied nanoparticle structures.[40]

In Table 2 and Fig. 5(a), the detected elements in the XPS measurements are depicted, Fe, O, C as components of the nanoparticles and Si, Na probably due to the microscopy glass support. Similar results were obtained by EDX.

In the Fig. 5(b-d), the high resolution XPS spectra for Fe2p, O1s and C1s of the MNP-CA sample are presented. In the high-resolution XPS spectra of

Fe2p, the Fe2p3/2 and Fe2p1/2 peaks with binding energies at 710.78 and 724.38 eV, respectively could be attributed to magnetite.[41, 42] In addition, the Fe2p spectrum has also two small satellite peaks at 719.25 and 732.85 eV that correspond to maghemite presence, indicating that the particles are composed of a mixture of iron oxides.

The high-resolution oxygen O1s spectrum of the MNP-CA sample is shown in Fig. 5(c). The O1s peak can be fitted using four sub-peaks. The peak at 530.27 eV is assigned to the Fe-O bond[43] and the one at 531.4 eV to the FeOOH species formed during the irradiation process.[44] The peak centered at 532.15 is specific for the COOH groups or carbonate species and the one at 532.88 eV can be attributed to the Si-OH bond[45] (from the glass substrate). The high resolution spectra of the C1s can be explained using four sub-peaks at 285 eV (C-C, C-H), at 285.47 eV (CH_2-CO), at 286.81 eV (C-OH) and 288.83 eV (C=O, C-O) corresponding to the presence of citric acid. No C=C or other bonds indicating possible decomposition products[35] of the organic phase are detected.

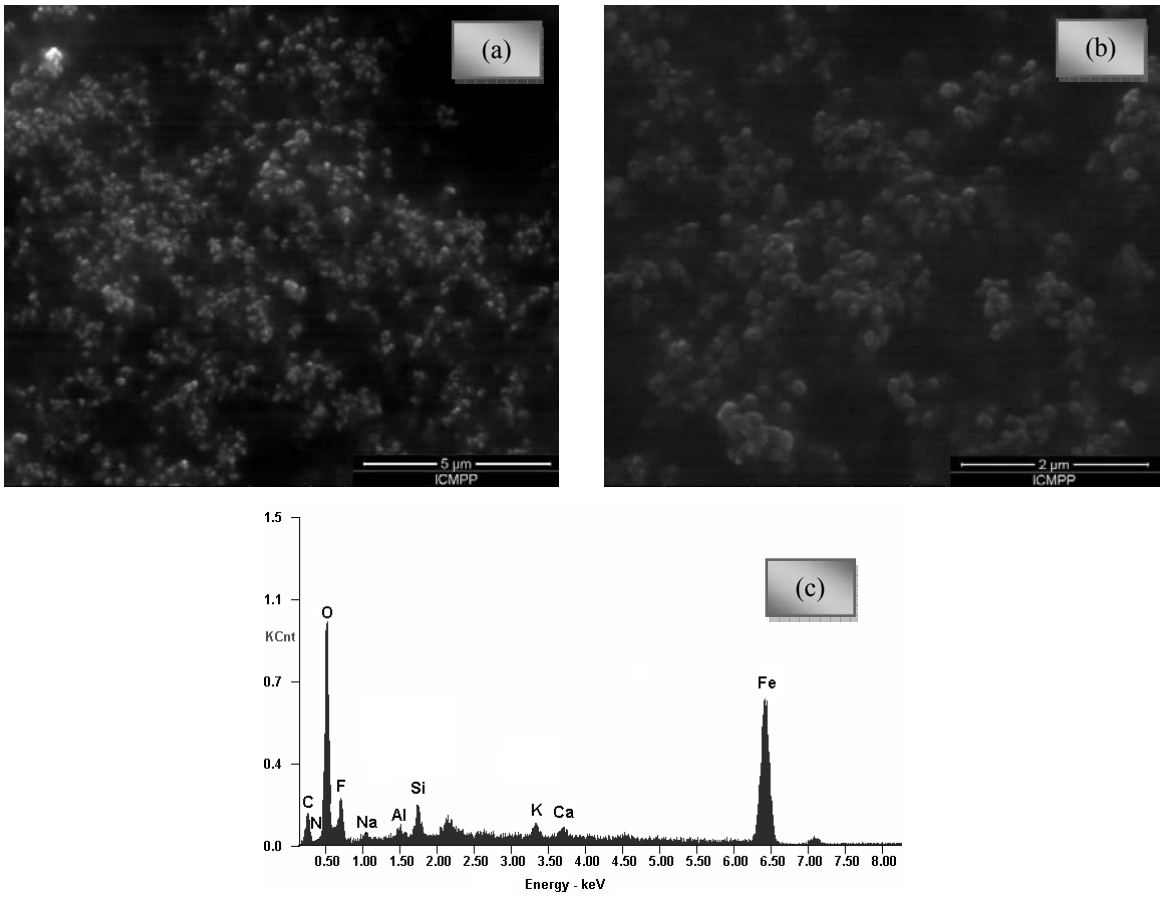

Fig. 3 – SEM micrographs of iron oxide-citric acid nanoparticles (MNP-CA) (a) scale 5 µm, (b) scale 2 µm. (c) EDX spectra and elemental composition of particles produced by laser ablation in citric acid solution.

Table 2

Elemental composition of MNP-CA nanoparticles as obtained by EDX and XPS (values in at%)

	Na	**Fe**	**O**	**N**	**C**	**Si**	**F**
EDX	0.99	6.56	48.82	3.06	28.89	2.03	8.93
XPS	0.73	7.83	33.82	0.97	50.16	6.49	0

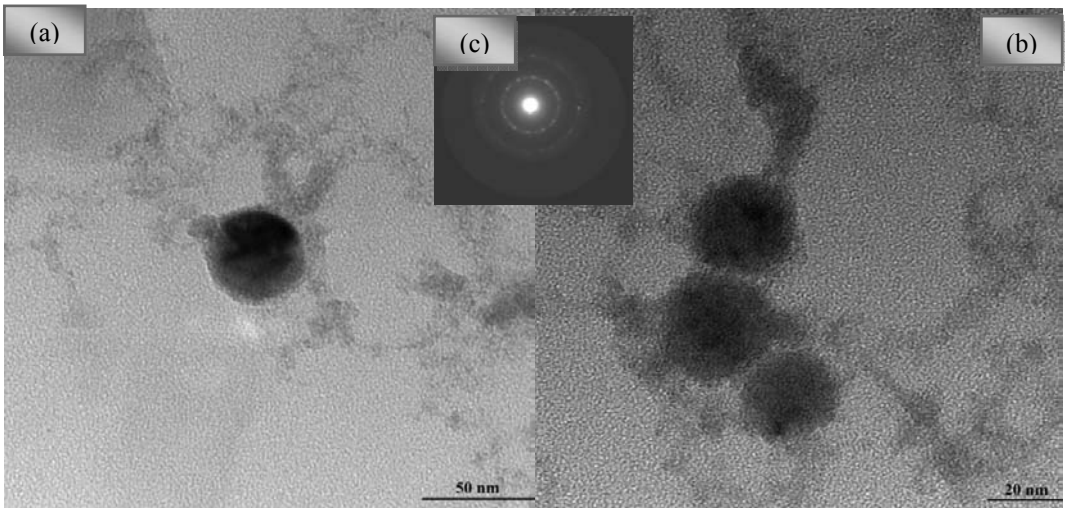

Fig. 4 – (a, b) TEM micrographs and (c) electron diffraction pattern for MNP-CA.

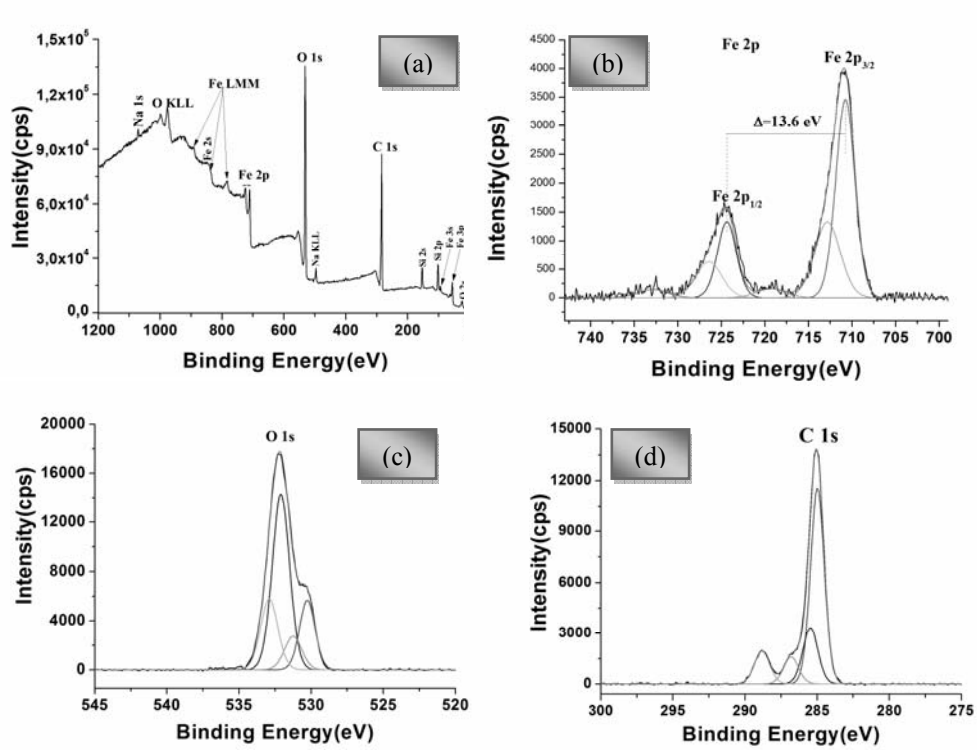

Fig. 5 – (a) XPS wide scan for MNP-CA. High-resolution XPS spectra of (b) iron Fe2p, (c) O1s and (d) C1s for MNP-CA nanoparticles.

Fourier Transform Infrared Spectroscopy (FTIR)

More information about the chemical composition of the nanoparticles was obtained by comparing the FTIR spectrum of pure citric acid with that of purified nanoparticles. Fig. 6 presents the FTIR spectra of the pure citric acid (a) and that of the iron oxide nanoparticles covered with citric acid (b). The intense band at approximately 3460 cm^{-1} can be assigned to the structural -OH groups of the citric acid and to the presence of water traces. The peak at 1728 cm^{-1} is attributed to the carbonyl C=O asymmetric stretching in the –COOH functional group of the citric acid. In the case of the iron oxide nanoparticles covered with citric acid the peak is shifted to 1618 cm^{-1} indicating the binding of the citric acid to the surface of the particles by chemical sorption of the carboxylate ions;[46,47] the carboxylate ion formation renders a partial single bond character to the carbonylic group, thus determining a weakening in the C=O bond and a shift to 1618 cm^{-1} respectively.[48]

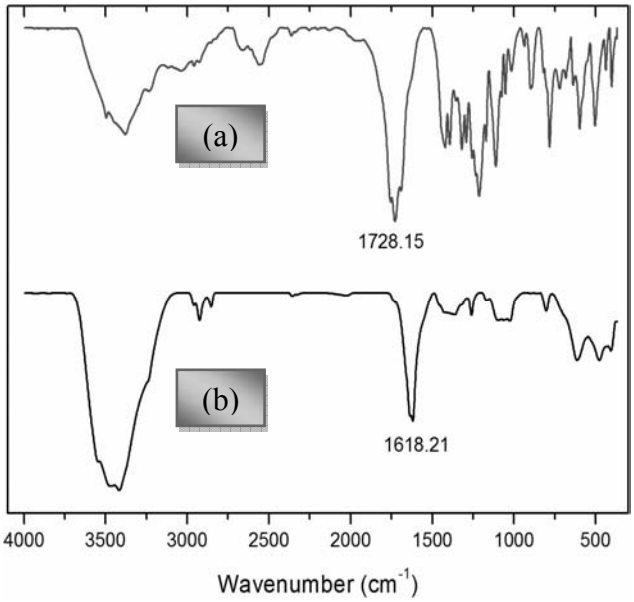

Fig. 6 – FTIR spectra of the pure citric acid (a) and of MNP-CA (b).

CONCLUSIONS

Iron oxides magnetic particles with nanometric sizes are successfully synthesized by laser ablation of iron in liquid and are stabilized by the citric acid present in the ablation medium. The particles obtained have spherical shape and have unimodal size distribution with average size of ≈ 60 nm. Chemical analysis indicates them to be a mixture of iron oxides (including bio-friendly maghemite), stabilized by the presence of citric acid in the form of carboxylate ions bound on their surface.

The work presented here can be followed by the conjugation of the produced nanoparticles with various biologic molecules and study their effect/interaction with biological target. This way, the formation of citric acid-coated magnetic nanoparticles offers an alternative way to obtain biocompatible magnetic nanoconjugates with applications in medicine.

Acknowledgements: This work was supported by a grant of the Roumanian National Authority for Scientific Research, CNCS – UEFISCDI, project number PN-II-RU-TE-2011-3-0174.

REFERENCES

1. P. Tartaj, M. d. P. Morales, S. Veintemillas-Verdaguer, T. González-Carreño and C. J. Serna, *J. Phys. D: Appl. Phys.*, **2003**, *36*, R182-R197.
2. S. P. Gubin, Y. A. Koksharov, G. B. Khomutov and G. Y. Yurkov, *Russ. Chem. Rev.*, **2005**, *74*, 489-520.
3. A. K. Gupta and M. Gupta, *Biomater.*, **2005**, *26*, 3995-4021.
4. N. A. Frey, S. Peng, K. Cheng and S. Sun, *Chem.l Soc. Rev.*, **2009**, *38*, 2532-2542.
5. R. Hao, R. Xing, Z. Xu, Y. Hou, S. Gao and S. Sun, *Adv. Mater.*, **2010**, *22*, 2729-2742.
6. B. Kateb, K. Chiu, K. L. Black, V. Yamamoto, B. Khalsa, J. Y. Ljubimova, H. Ding, R. Patil, J. A. Portilla-Arias, M. Modo, D. F. Moore, K. Farahani, M. S. Okun, N. Prakash, J. Neman, D. Ahdoot, W. Grundfest, S. Nikzad and J. D. Heiss, *NeuroImage*, **2011**, *54, Supplement 1*, S106-S124.
7. A. Durdureanu-Angheluta, A. Dascalu, A. Fifere, A. Coroaba, L. Pricop, H. Chiriac, V. Tura, M. Pinteala and B. C. Simionescu, *J. Magn. Magn. Mater.*, **2012**, *324*, 1679-1689.
8. A. Durdureanu-Angheluta, R. Ardeleanu, M. Pinteala, V. Harabagiu, H. Chiriac and B. C. Simionescu, *Digest J. Nanomater. Biostruct.*, **2008**, *3*, 33-40.
9. A. Durdureanu-Angheluta, L. Pricop, I. Stoica, C. A. Peptu, A. Dascalu, N. Marangoci, F. Doroftei, H. Chiriac, M. Pinteala and B. C. Simionescu, *J. Magn. Magn. Mater.*, **2010**, *322*, 2956-2968.
10. G. W. Yang, *Progr. Mater. Sci.*, **2007**, *52*, 648-698.
11. N. V. Tarasenko and A. V. Butsen, *Quantum Electron.*, **2010**, *40*, 986.
12. H. Zeng, X.-W. Du, S. C. Singh, S. A. Kulinich, S. Yang, J. He and W. Cai, *Adv. Funct. Mater.*, **2012**, *22*, 1333-1353.
13. S. C. Singh and H. Zeng, *Sci. Adv. Mater.*, **2012**, *4*, 368-390.
14. T. Sasaki, Y. Shimizu and N. Koshizaki, *J. Photochem. Photobiol. A: Chemistry*, **2006**, *182*, 335-341.
15. P. Liu, W. Cai and H. Zeng, *J. Phys. Chem. C*, **2008**, *112*, 3261-3266.
16. P. P. Patil, D. M. Phase, S. A. Kulkarni, S. V. Ghaisas, S. K. Kulkarni, S. M. Kanetkar, S. B. Ogale and V. G. Bhide, *Phys. Rev. Lett.* , **1987**, *58*, 238-241.
17. S. B. Ogale, P. P. Patil, D. M. Phase, Y. V. Bhandarkar, S. K. Kulkarni, S. Kulkarni, S. V. Ghaisas, S. M. Kanetkar, V. G. Bhide and S. Guha, *Phys. Rev. B*, **1987**, *36*, 8237-8250.
18. S. B. Ogale, *Thin Solid Films*, **1988**, *163*, 215-227.
19. V. Amendola, M. Meneghetti, G. Granozzi, S. Agnoli, S. Polizzi, P. Riello, A. Boscaini, C. Anselmi, G. Fracasso, M. Colombatti, C. Innocenti, D. Gatteschi and C. Sangregorio, *J. Mater. Chem.*, **2011**, *21*, 3803-3813.

20. V. Amendola, P. Riello, S. Polizzi, S. Fiameni, C. Innocenti, C. Sangregorio and M. Meneghetti, *J. Mater. Chem.*, **2011**, *21*, 18665-18673.
21. V. Amendola, P. Riello and M. Meneghetti, *J. Phys. Chem. C*, **2011**, *115*, 5140-5146.
22. L. Franzel, M. F. Bertino, Z. J. Huba and E. E. Carpenter, *Appl. Surf. Sci.*, **2012**, *261*, 332-336.
23. S. Mollah, S. J. Henley and S. R. P. Silva, *Nanotechnol.*, **2008**, *19*, 205604.
24. S. Mollah, S. J. Henley, C. E. Giusca and S. R. P. Silva, *Integrated Ferroelectrics*, **2010**, *119*, 45-54.
25. W. Zhang and Z. Jin, *Sci. China Ser. B: Chemistry*, **2004**, *47*, 159-165.
26. J. B. Park, S. H. Jeong, M. S. Jeong, J. Y. Kim and B. K. Cho, *Carbon*, **2008**, *46*, 1369-1377.
27. Y. Vitta, V. Piscitelli, A. Fernandez, F. Gonzalez-Jimenez and J. Castillo, *Chem. Phys. Lett.*, **2011**, *512*, 96-98.
28. I. A. Sukhov, A. V. Simakin, G. A. Shafeev, G. Viau and C. Garcia, *Quantum Electron.*, **2012**, *42*, 453-456.
29. K. Y. Niu, J. Yang, S. A. Kulinich, J. Sun and X. W. Du, *Langmuir*, **2010**, *26*, 16652-16657.
30. K. Y. Niu, J. Yang, S. A. Kulinich, J. Sun, H. Li and X. W. Du, *J. Am. Chem. Soc.*, **2012**, *132*, 9814-9819.
31. T. Goetze, C. Gansau, N. Buske, M. Roeder, P. Görnert and M. Bahr, *J. Magn. Magn. Mater.*, **2002**, *252*, 399-402.
32. Y. Sahoo, A. Goodarzi, M. T. Swihart, T. Y. Ohulchanskyy, N. Kaur, E. P. Furlani and P. N. Prasad, *J. Phys. Chem. B*, **2005**, *109*, 3879-3885.
33. M. Lattuada and T. A. Hatton, *Langmuir*, **2006**, *23*, 2158-2168.
34. E. Cheraghipour, A. M. Tamaddon, S. Javadpour and I. J. Bruce, *J. Magn. Magn. Mater.*, **2013**, *328*, 91-95.
35. M. M. Barbooti and D. A. Al-Sammerrai, *Thermochim. Acta*, **1986**, *98*, 119-126.
36. P. Calandra, D. Lombardo, F. Neri, A. Ruggirello, S. Trusso and V. T. Liveri, *Mater. Lett.*, **2010**, *64*, 576-579.
37. N. G. Semaltianos, S. Logothetidis, N. Frangis, I. Tsiaoussis, W. Perrie, G. Dearden and K. G. Watkins, *Chem. Phys. Lett.*, **2010**, *496*, 113-116.
38. J. A. Creighton and D. G. Eadon, *J. Chem. Soc., Faraday Trans.*, **1991**, *87*, 3881-3891.
39. Y. Z. Hamada, B. L. Carlson and J. T. Shank, *Synth. React. Inorg. Met.-Org. Chem*, **2003**, *33*, 1425-1440.
40. C. Chan, H. Gallard and P. Majewski, *J. Nanopart. Res.*, **2012**, *14*, 1-11.
41. D. Zhang, Z. Liu, S. Han, C. Li, B. Lei, M. P. Stewart, J. M. Tour and C. Zhou, *Nano Lett.*, **2004**, *4*, 2151-2155.
42. T. Yamashita and P. Hayes, *Appl. Surf. Sci.*, **2008**, *254*, 2441-2449.
43. P. J. Linstrom and W.G. Mallard (Eds.), "NIST Chemistry WebBook, NIST Standard Reference Database Number 69", National Institute of Standards and Technology, Gaithersburg MD, 20899, http://webbook.nist.gov, (retrieved December 4, 2013).
44. W. Temesghen and P. Sherwood, *Anal. Bioanal. Chem.*, **2002**, *373*, 601-608.
45. J. F. Moulder, W. F. Stickle, P. E. Sobol and K. Bomben, "Handbook of X-ray Photoelectron Spectroscop 2nd ed.", Perkin-Elmer Corporation (Physical Electronics), 1992.
46. M. Răcuciu, D. E. Creangă and A. Airinei, *Eur. Phys. J. E*, **2006**, *21*, 117-121.
47. Q. Lan, C. Liu, F. Yang, S. Liu, J. Xu and D. Sun, *J. Colloid Interface Sci.*, **2007**, *310*, 260-269.
48. S. Nigam, K. C. Barick and D. Bahadur, *J. Magn. Magn. Mater.*, **2011**, *323*, 237-243.